mathematics

MDPI

Article

A Fast Singular Boundary Method for the Acoustic Design Sensitivity Analysis of Arbitrary Two- and Three-Dimensional Structures

Liyuan Lan [1], Suifu Cheng [1], Xiatao Sun [2], Weiwei Li [3], Chao Yang [4,*] and Fajie Wang [1,*]

[1] National Engineering Research Center for Intelligent Electrical Vehicle Power System, College of Mechanical and Electrical Engineering, Qingdao University, Qingdao 266071, China
[2] School of Engineering and Applied Science, University of Pennsylvania, Philadelphia, PA 19104, USA
[3] School of Transportation and Vehicle Engineering, Shandong University of Technology, Zibo 255049, China
[4] College of Materials Science and Engineering, Qingdao University, Qingdao 266071, China
* Correspondence: yangchao@qdu.edu.cn (C.Y.); wfj88@qdu.edu.cn (F.W.)

Abstract: This paper proposes a fast meshless scheme for acoustic sensitivity analysis by using the Burton–Miller-type singular boundary method (BM-SBM) and recursive skeletonization factorization (RSF). The Burton–Miller formulation was adopted to circumvent the fictitious frequency that occurs in external acoustic analysis, and then the direct differentiation method was used to obtain the sensitivity of sound pressure to design variables. More importantly, RSF was employed to solve the resultant linear system obtained by the BM-SBM. RSF is a fast direct factorization technique based on multilevel matrix compression, which allows fast factorization and application of the inverse in solving dense matrices. Firstly, the BM-SBM is a boundary-type collocation method that is a straightforward and accurate scheme owing to the use of the fundamental solution. Secondly, the introduction of the fast solver can effectively reduce the requirement of computer memory and increase the calculation scale compared to the conventional BM-SBM. Three numerical examples including two- and three-dimensional geometries indicate the precision and efficiency of the proposed fast numerical technique for acoustic design sensitivity analysis associated with large-scale and complicated structures.

Keywords: recursive skeletonization factorization; Burton–Miller-type singular boundary method; fast solver; fundamental solution; acoustic design sensitivity

MSC: 65N35; 76Q05

Citation: Lan, L.; Cheng, S.; Sun, X.; Li, W.; Yang, C.; Wang, F. A Fast Singular Boundary Method for the Acoustic Design Sensitivity Analysis of Arbitrary Two- and Three-Dimensional Structures. *Mathematics* **2022**, *10*, 3817. https://doi.org/10.3390/math10203817

Academic Editor: Yury Shestopalov

Received: 16 September 2022
Accepted: 12 October 2022
Published: 16 October 2022

1. Introduction

In recent years, various methods [1–4] have been proposed to address acoustic problems, such as transient acoustic wave propagation in unbounded domains [5], acoustic transmission across multilayered construction [6], wave diffusion in unbounded domains [7], and acoustic sensitivity analysis [8]. For these problems, numerical simulation plays an irreplaceable role. Common methods for the analysis of acoustic problems include the finite element method (FEM) [9,10], the boundary element method (BEM) [11,12], and some alternative meshless/mesh-free methods. Meshless methods can reduce or even eliminate the tasks of grid generation and numerical integration. Therefore, many scholars and engineers have developed numerous meshless approaches, such as the element-free Galerkin method [13,14], the exponential basis function method [15,16], the localized semi-analytical meshless collocation method [17–19], the method of fundamental solutions (MFS) [20,21], and the singular boundary method (SBM) [22].

Among the above methods, the SBM is a semi-analytical and boundary-type meshless approach using fundamental solutions, which is mathematically simple, numerically accurate, and easy to program. Unlike the MFS, the SBM avoids the singularity of fundamental

solutions by introducing the origin intensity factor (OIF), and circumvents the fictitious boundary issue in the traditional MFS. To overcome the influence of the fictitious eigenfrequency issue, the BM-SBM was proposed to deal with sound scattering and radiation [23,24]. Up to now, this scheme has been successfully applied to acoustic simulations [25–27], heat conduction analysis [28,29], electromagnetic problems [30], and other domains.

Similar to the traditional boundary-type methods [31–33], the resultant matrix of the BM-SBM is a dense matrix. Assuming that the number of boundary nodes is N, the storage process needs to occupy the memory of $O(N^2)$, and the operations of $O(N^3)$ are required in the direct calculation. Therefore, insufficient memory and time-consuming computation are often encountered when solving large-scale problems. In order to reduce the calculation time and increase the calculation scale, some scholars have introduced various fast algorithms. The fast multipole (FM) and adaptive cross approximation (ACA) have been used to establish a series of new fast algorithms, such as the fast multipole BEM (FM-BEM) [34–36], the fast multipole MFS (FMM-MFS) [37], the ACA-BEM [38], and the ACA-MFS [39]. Moreover, the ACA-BEM has also been successfully applied to the solution of acoustic sensitivity. The SBM, which draws inspiration from the boundary element technique, has also been combined with fast algorithms to address large-scale problems. Qu et al. [40,41] proposed the fast multipole accelerated SBM (FMM-SBM) to solve large-scale Helmholtz problems, increasing the computational scale of boundary nodes to more than one million. Wei et al. [42] developed an adaptive cross approximation SBM (ACA-SBM) to simulate 2D steady-state heat transfer problems. Li et al. [43–45] developed a precorrected-FFT SBM (PFFT-SBM) to address large-scale 3D Laplace problems, Helmholtz problems, and high-frequency acoustic radiation and scattering problems. Li et al. [46,47] proposed a fast SBM for solving the 2D steady-state heat conduction problem and large-scale 3D potential problem.

This paper aims to present a fast formulation of the BM-SBM for analyzing the acoustic sensitivity of 2D and 3D complex structures. In our earlier works [48,49], we built a BM-SBM framework for acoustic design sensitivity analysis. Benchmark numerical examples confirmed the accuracy and effectiveness of the method. However, the approach still faces the challenge of addressing a large-scale structure. Recursive skeletonization factorization (RSF) [50,51] is a fast and direct scheme based on multilevel matrix compression, and has been successfully applied to various problems. In this paper, RSF is adopted to solve the resultant system of the BM-SBM, and then a new fast method called the RSF-BM-SBM is proposed. Compared with the original BM-SBM, the calculation time is greatly reduced, and the computational scale is significantly increased.

The rest of this paper is organized as follows. In Section 2, we briefly introduce the acoustic sensitivity formula of the BM-SBM and the empirical formula of the OIFs. In Section 3, recursive skeletonization factorization is shown to solve the linear system formed in the sensitivity analysis using the BM-SBM. In Section 4, three examples, including classical models and a complex car model, are demonstrated to verify the accuracy and efficiency of the proposed RSF-BM-SBM for acoustic sensitivity analysis. In Section 5, some conclusions are drawn.

2. Burton–Miller-Type Singular Boundary Method for Acoustic Sensitivity

2.1. Acoustic Sensitivity Analysis

We consider an external sound field problem in two- and three-dimensional spaces, which can be described by the following Helmholtz equation [48,49]:

$$\nabla^2 u(\boldsymbol{x}) + k^2 u(\boldsymbol{x}) = 0 \, , \boldsymbol{x} \in \Omega \tag{1}$$

with the following Dirichlet and Neumann boundary conditions:

$$u(\boldsymbol{x}) = \overline{u}(\boldsymbol{x}), \boldsymbol{x} \in \Gamma_u, \tag{2}$$

$$\frac{\partial u(\boldsymbol{x})}{\partial \boldsymbol{n}_{\boldsymbol{x}}} = \mathrm{i}\rho\omega\overline{v}(\boldsymbol{x}), \boldsymbol{x} \in \Gamma_q, \tag{3}$$

where ∇^2 represents the Laplace operator; $k = \omega/c$ is the wave number; ω is the angular frequency; c is the speed of sound in the propagating medium; and $\overline{u}(\boldsymbol{x})$ and $\overline{v}(\boldsymbol{x})$ are the sound pressure and the normal vibration velocity on Γ_u and Γ_q, respectively.

Considering sound propagation in an infinite field, the sound pressure should satisfy the Sommerfeld radiation condition at infinity:

$$\lim_{r\to\infty} r^{\frac{1}{2}(d-1)}\left(\frac{\partial u(\boldsymbol{x})}{\partial r} - \mathrm{i}ku(\boldsymbol{x})\right) = 0 \tag{4}$$

where d is the spatial dimension (d = 2, 3) and r is the distance between point $\boldsymbol{x}$ and the sound field's center. The fundamental solution employed in the BM-SBM automatically satisfies the aforementioned requirements; therefore, no additional handling is necessary in the numerical computation.

For acoustic sensitivity analysis, the most important thing is to obtain the gradient of the objective function with respect to the design variables. In many applications, the objective function is sound pressure, and the design variables are size, wave number, or frequency.

2.2. Burton–Miller-Type Singular Boundary Method

Assuming the total number of boundary nodes is N, the BM-SBM formulas can be given by [49]:

$$u(\boldsymbol{x}_i) = \sum_{\substack{j=1 \\ i\neq j}}^{N} \alpha_j\left(G(\boldsymbol{x}_i,\boldsymbol{s}_j) + \lambda E(\boldsymbol{x}_i,\boldsymbol{s}_j)\right) + \alpha_i u_{BM},\ \boldsymbol{x}_i \in \Gamma_u,\ \boldsymbol{s}_j \in \Gamma \tag{5}$$

$$\frac{\partial u(\boldsymbol{x}_i)}{\partial \boldsymbol{n}_x} = \sum_{\substack{j=1 \\ i\neq j}}^{N} \alpha_j\left(F(\boldsymbol{x}_i,\boldsymbol{s}_j) + \lambda H(\boldsymbol{x}_i,\boldsymbol{s}_j)\right) + \alpha_i q_{BM},\ \boldsymbol{x}_i \in \Gamma_q,\ \boldsymbol{s}_j \in \Gamma \tag{6}$$

$$E(\boldsymbol{x}_i,\boldsymbol{s}_j) = \frac{\partial G(\boldsymbol{x}_i,\boldsymbol{s}_j)}{\partial \boldsymbol{n}_s},\ F(\boldsymbol{x}_i,\boldsymbol{s}_j) = \frac{\partial G(\boldsymbol{x}_i,\boldsymbol{s}_j)}{\partial \boldsymbol{n}_x},\ H(\boldsymbol{x}_i,\boldsymbol{s}_j) = \frac{\partial^2 G(\boldsymbol{x}_i,\boldsymbol{s}_j)}{\partial \boldsymbol{n}_s \partial \boldsymbol{n}_x} \tag{7}$$

where $\lambda = \frac{\mathrm{i}}{k+1}$ is a complex number [24]; α_j is the unknown coefficient; and $\boldsymbol{x}_i$ and $\boldsymbol{s}_j$ denote ith boundary node and jth source point, respectively. u_{BM} and q_{BM} are the OIFs, which can be computed by the following formulas [52,53]:

$$u_{BM} = u_{ii} - \lambda \sum_{\substack{j=1 \\ j\neq i}}^{N} \zeta_{ji} \frac{\partial G_0(\boldsymbol{x}_i,\boldsymbol{s}_j)}{\partial \boldsymbol{n}_s} \tag{8}$$

$$q_{BM} = q_{ii} + \lambda \left(\frac{k^2}{2} u_{ii} - \sum_{\substack{j=1 \\ j\neq i}}^{N} \zeta_{ji} \frac{\partial^2 G_0(\boldsymbol{x}_i,\boldsymbol{s}_j)}{\partial \boldsymbol{n}_s \partial \boldsymbol{n}_x} \right) \tag{9}$$

where u_{ii} and q_{ii} are given in Refs. [24,48], and $G_0(\boldsymbol{x}_i,\boldsymbol{s}_j)$ is the fundamental solution of the Laplace equation. $G_0(\boldsymbol{x}_i,\boldsymbol{s}_j) = -\frac{\ln|\boldsymbol{x}_i-\boldsymbol{s}_j|}{2\pi}$ for 2D problems; $G_0(\boldsymbol{x}_i,\boldsymbol{s}_j) = \frac{1}{4\pi|\boldsymbol{x}_i-\boldsymbol{s}_j|}$ for 3D problems.

Substituting the boundary conditions into Equations (5) and (6), the following system of equations can be obtained:

$$\mathbf{M}\boldsymbol{\alpha} = \mathbf{b} \tag{10}$$

where $\mathbf{M}_{N\times N}$ is the coefficient matrix, $\boldsymbol{\alpha}_{N\times 1}$ is the undetermined coefficient vector, and $\mathbf{b}_{N\times 1}$ is the known vector. The matrix $\mathbf{M}$ is generated from Burton–Miller-type formulation (a combination of single- and double-layer potentials), and its condition number is related to the number of nodes. Since the method is implemented by MATLAB programming, the condition number of the matrix can be viewed by the routine *cond*(M). By solving Equation (10), $\boldsymbol{\alpha}$ can be obtained. After that, the following formulas can be employed to determine the sound pressure and normal derivative at point $\boldsymbol{x}$:

$$u(\boldsymbol{x}) = \sum_{j=1}^{N} \alpha_j \big(G(\boldsymbol{x}, \boldsymbol{s}_j) + \lambda E(\boldsymbol{x}, \boldsymbol{s}_j)\big) \tag{11}$$

$$q(\boldsymbol{x}) = \sum_{j=1}^{N} \alpha_j \big(F(\boldsymbol{x}, \boldsymbol{s}_j) + \lambda H(\boldsymbol{x}, \boldsymbol{s}_j)\big) \tag{12}$$

Based on the formulas mentioned above, the direct differentiation approach can be used to compute the sensitivities:

$$\dot{u}(\boldsymbol{x}) = \sum_{j=1}^{N} \begin{bmatrix} \dot{\alpha}_j \big(G(\boldsymbol{x}, \boldsymbol{s}_j) + \lambda E(\boldsymbol{x}, \boldsymbol{s}_j)\big) \\ +\alpha_j \Big(\dot{G}(\boldsymbol{x}, \boldsymbol{s}_j) + \dot{\lambda} E(\boldsymbol{x}, \boldsymbol{s}_j) + \lambda \dot{E}(\boldsymbol{x}, \boldsymbol{s}_j)\Big) \end{bmatrix} \tag{13}$$

$$\dot{q}(\boldsymbol{x}) = \sum_{j=1}^{N} \begin{bmatrix} \dot{\alpha}_j \big(F(\boldsymbol{x}, \boldsymbol{s}_j) + \lambda H(\boldsymbol{x}, \boldsymbol{s}_j)\big) \\ +\alpha_j \Big(\dot{F}(\boldsymbol{x}, \boldsymbol{s}_j) + \dot{\lambda} H(\boldsymbol{x}, \boldsymbol{s}_j) + \lambda \dot{H}(\boldsymbol{x}, \boldsymbol{s}_j)\Big) \end{bmatrix} \tag{14}$$

where the superscript $(\dot{\cdot})$ denotes the differentiation of a function. For the differentiation calculation in the right hand sides of the above equations, one can refer to Ref. [48].

3. Recursive Skeletonization Factorization

Recursive skeleton factorization is a fast direct solver which allows fast factorization and application of the inverse in the process of solving asymmetric dense matrices.

3.1. Interpolative Decomposition

The present paper adopts interpolative decomposition (ID) to compress the low-rank blocks [46,54]. If the submatrix $\mathbf{M}_{pq} \in \mathbb{R}^{m\times n}$ of $\mathbf{M}$ is a matrix of rank $h \leq \min(m, n)$, then there exist $\mathbf{R}_q \in \mathbb{R}^{h\times(n-t)}$ such that $\mathbf{M}_{pq'} \approx \mathbf{M}_{pq''}\mathbf{R}_q$. It should be pointed out that m and n denote the dimension of the matrix $\mathbf{M}$, which are set as $m = n = N$. Here, p and q represent ordered sets of indices, q' and q'' denote the skeleton and redundant indices, and they satisfy the following relationships: $q = q' \cup q''$ and $|q''| = h$. If $\mathbf{R}_q$ satisfy $\mathbf{M}_{pq'} = \mathbf{M}_{pq''}\mathbf{R}_q$, then

$$\begin{bmatrix} \mathbf{M}_{pq'} & \mathbf{M}_{pq''} \end{bmatrix} \begin{bmatrix} \mathbf{I} & \\ -\mathbf{R}_q & \mathbf{I} \end{bmatrix} = \begin{bmatrix} 0 & \mathbf{M}_{pq''} \end{bmatrix} \tag{15}$$

It should be pointed out that ID is commonly applied to cases with an error matrix $\mathbf{E}$, i.e., $\mathbf{M}_{pq'} = \mathbf{M}_{pq''}\mathbf{R}_q + \mathbf{E}$, in which $||\mathbf{E}|| \sim \sigma_{h+1}(\mathbf{M})$, and $\sigma_{h+1}(\mathbf{M})$ stands for the $(h+1)$th-largest singular value of $\mathbf{M}$. In this regard, ID can be employed to select h adaptively, so that $||\mathbf{E}|| \leq \varepsilon ||\mathbf{M}||$ for a given tolerance $\varepsilon > 0$. In this paper, ID is achieved by a random sampling scheme [54], which only requires $O\big(mn\log(h) + h^2 n\big)$ operations.

3.2. Skeletonization

In this subsection, ID is adopted to compress a matrix with low-rank off-diagonal blocks. We consider a block matrix $\mathbf{M}$ with index sets p and q:

$$\mathbf{M} = \begin{bmatrix} \mathbf{M}_{pp} & \mathbf{M}_{pq} \\ \mathbf{M}_{qp} & \mathbf{M}_{qq} \end{bmatrix} \tag{16}$$

where $\mathbf{M}_{pq}$ and $\mathbf{M}_{qp}$ are low-rank submatrices. After applying ID to $\mathbf{M}$ with $p = p' \cup p''$, we obtain

$$\mathbf{M} = \begin{bmatrix} \mathbf{M}_{p'p'} & \mathbf{M}_{p'p''} & \mathbf{M}_{p'q} \\ \mathbf{M}_{p''p'} & M_{p''p''} & \mathbf{M}_{p''q} \\ \mathbf{M}_{qp'} & \mathbf{M}_{qp''} & \mathbf{M}_{qq} \end{bmatrix} \tag{17}$$

Let

$$\mathbf{Q}_p = \begin{bmatrix} \mathbf{I} & & \\ -\mathbf{R}_p & \mathbf{I} & \\ & & \mathbf{I} \end{bmatrix} \tag{18}$$

and then

$$\mathbf{Q}_p^{\mathrm{T}} \mathbf{M} \mathbf{Q}_p \approx \begin{bmatrix} \mathbf{N}_{p'p'} & \mathbf{N}_{p'p''} & \\ \mathbf{N}_{p''p'} & \mathbf{M}_{p''p''} & \mathbf{M}_{p''q} \\ & \mathbf{M}_{qp''} & \mathbf{M}_{qq} \end{bmatrix} \tag{19}$$

where

$$\mathbf{N}_{p'p'} = \mathbf{M}_{p'p'} - \mathbf{R}_p^{\mathrm{T}} \mathbf{M}_{p'',p'} - \mathbf{M}_{p'p''} \mathbf{R}_p + \mathbf{R}_p^{\mathrm{T}} \mathbf{M}_{p''p''} \mathbf{R}_p \tag{20}$$

$$\mathbf{N}_{p'p''} = \mathbf{M}_{p'p''} - \mathbf{R}_p^{\mathrm{T}} \mathbf{M}_{p''p''}, \ \ \mathbf{N}_{p''p'} = \mathbf{M}_{p''p'} - \mathbf{M}_{p''p''} \mathbf{R}_p \tag{21}$$

Supposing $\mathbf{N}_{p'p'}$ is a nonsingular matrix, and $\mathbf{N}_{p'p''}$ can be decomposed into $\mathbf{L}_{p'} \mathbf{D}_{p'} \mathbf{U}_{p'}$ ($\mathbf{D}_{p'}$ is a diagonal matrix; $\mathbf{L}_{p'}$ and $\mathbf{U}_{p'}$ are unit triangular matrices), we obtain

$$\boldsymbol{s}_{p'}^{\mathrm{T}} \mathbf{Q}_p^{\mathrm{T}} \mathbf{M} \mathbf{Q}_p \mathbf{T}_{p'} \approx \begin{bmatrix} \mathbf{D}_{p'} & & \\ & \mathbf{N}_{p'',p''} & \mathbf{M}_{p'',q} \\ & \mathbf{M}_{q,p''} & \mathbf{M}_{q,q} \end{bmatrix} \equiv \Psi_p(\mathbf{M}) \tag{22}$$

where $\Psi_p(\cdot)$ is called the skeletonization operator, and

$$\boldsymbol{s}_{p'}^{\mathrm{T}} = \begin{bmatrix} \mathbf{I} & & \\ -\mathbf{N}_{p''p'} \mathbf{U}_{p'}^{-1} \mathbf{D}_{p'}^{-1} & \mathbf{I} & \\ & & \mathbf{I} \end{bmatrix} \begin{bmatrix} \mathbf{L}_{p'}^{-1} & & \\ & \mathbf{I} & \\ & & \mathbf{I} \end{bmatrix} \tag{23}$$

$$\mathbf{T}_{p'} = \begin{bmatrix} \mathbf{U}_{p'}^{-1} & & \\ & \mathbf{I} & \\ & & \mathbf{I} \end{bmatrix} \begin{bmatrix} \mathbf{I} & -\mathbf{D}_{p'}^{-1} \mathbf{L}_{p'}^{-1} \mathbf{N}_{p'p''} & \\ & \mathbf{I} & \\ & & \mathbf{I} \end{bmatrix} \tag{24}$$

$$\mathbf{N}_{p''p''} = \mathbf{M}_{p''p''} - \mathbf{N}_{p''p'} \mathbf{N}_{p'p'}^{-1} \mathbf{N}_{p'p''} \tag{25}$$

Considering a collection of disjoint index sets C, in which $\mathbf{M}_{c,c^C}$ and $\mathbf{M}_{c^C,c}$ are low-rank for any $c \in C$, $\Psi_C(\mathbf{M})$ can be decomposed into

$$\Psi_C(\mathbf{M}) \approx \mathbf{U}^{\mathrm{T}} \mathbf{M} \mathbf{V} \tag{26}$$

where c^C denotes the complement of the index set c, $\mathbf{U} = \prod_{c \in C} \mathbf{Q}_c \mathbf{S}_{c'}$, and $\mathbf{V} = \prod_{c \in C} \mathbf{Q}_c \mathbf{T}_{c'}$.

3.3. Recursive Skeletonization Factorization (RSF)

Let C_j denote the collection of the skeleton index set at level j. We define the matrix at each level j by using $\mathbf{M}_j$. It should be noted that $\mathbf{M}_0 = \mathbf{M}$. Based on the skeletonization mentioned above, we have

$$\mathbf{M}_{j+1} = \Psi_{C_j}(\mathbf{M}_j) \approx \mathbf{U}_j^{\mathrm{T}} \mathbf{M}_j \mathbf{V}_j, \quad \mathbf{U}_j = \prod_{c \in C_j} \mathbf{Q}_c \mathbf{S}_{c'}, \quad \mathbf{V}_j = \prod_{c \in C_j} \mathbf{Q}_c \mathbf{T}_{c'} \tag{27}$$

By using RSF, each $\mathbf{U}_j$ and $\mathbf{V}_j$ are products of unit triangular matrices, and can be simply inverted and transposed. Then, according to the same principle, the factorization can be written as

$$\mathbf{M}_j \approx \mathbf{U}_{j-1}^{\mathrm{T}} \cdots \mathbf{U}_0^{\mathrm{T}} \mathbf{M} \mathbf{V}_0 \cdots \mathbf{V}_{j-1} \tag{28}$$

Note that the inversion and transposition of matrices $\mathbf{U}_j$ and $\mathbf{V}_j$ can be easily obtained, since they are products of unit triangular matrices. Therefore, $\mathbf{M}$ and $\mathbf{M}^{-1}$ can be calculated by

$$\mathbf{M} \approx \left[\mathbf{U}_0^{-1}\right]^{\mathrm{T}} \cdots \left[\mathbf{U}_{j-1}^{-1}\right]^{\mathrm{T}} \mathbf{M}_j \mathbf{V}_{j-1}^{-1} \cdots \mathbf{V}_0^{-1} \tag{29}$$

$$\mathbf{M}^{-1} \approx \mathbf{V}_0 \cdots \mathbf{V}_{j-1} \mathbf{M}_j \mathbf{U}_{j-1}^{\mathrm{T}} \cdots \mathbf{U}_0^{\mathrm{T}} \tag{30}$$

After obtaining $\mathbf{M}^{-1}$ from Equation (30), the unknown coefficient vector $\boldsymbol{\alpha}$ in Equation (10) can be acquired by the following formula:

$$\boldsymbol{\alpha} = \mathbf{M}^{-1} \mathbf{b} \tag{31}$$

4. Numerical Examples

Here, two benchmark examples are firstly investigated to demonstrate the accuracy of the RSF-BM-SBM, and then the feasibility and effectiveness of the method to solve large-scale problems are verified by calculating the sensitivity of a vehicle model. Assuming that the design variable t is divided into m equidistant nodes, the following relative-root-mean-square error (RRMSE) [24] is adopted to evaluate numerical error:

$$\mathrm{RRMSE} = \frac{\sqrt{\sum_{j=1}^{m} \left(\dot{u}_e(t_j) - \dot{u}_n(t_j)\right)^2}}{\sqrt{\sum_{j=1}^{m} \dot{u}_e(t_j)^2}} \tag{32}$$

where $\dot{u}_e$ and $\dot{u}_n$ denote the exact and numerical solutions of the acoustic sensitivity, respectively. In the following numerical calculation, we have fixed the air density and the sound speed to $\rho = 1.2\ \mathrm{kg/m^3}$ and $c = 341\ \mathrm{m/s}$.

In acoustic sensitivity analysis, the gradient of the objective function with respect to the design variables needs to be obtained. Taking the sound pressure p as the objective function, it can be expressed as $\frac{\partial p(\boldsymbol{x})}{\partial t}$, where t represents the design variable.

4.1. Example 1

In the first example, we consider an infinite pulsating cylinder [49] with radius $a = 0.1$ m, which can be reduced to a 2D problem as shown in Figure 1.

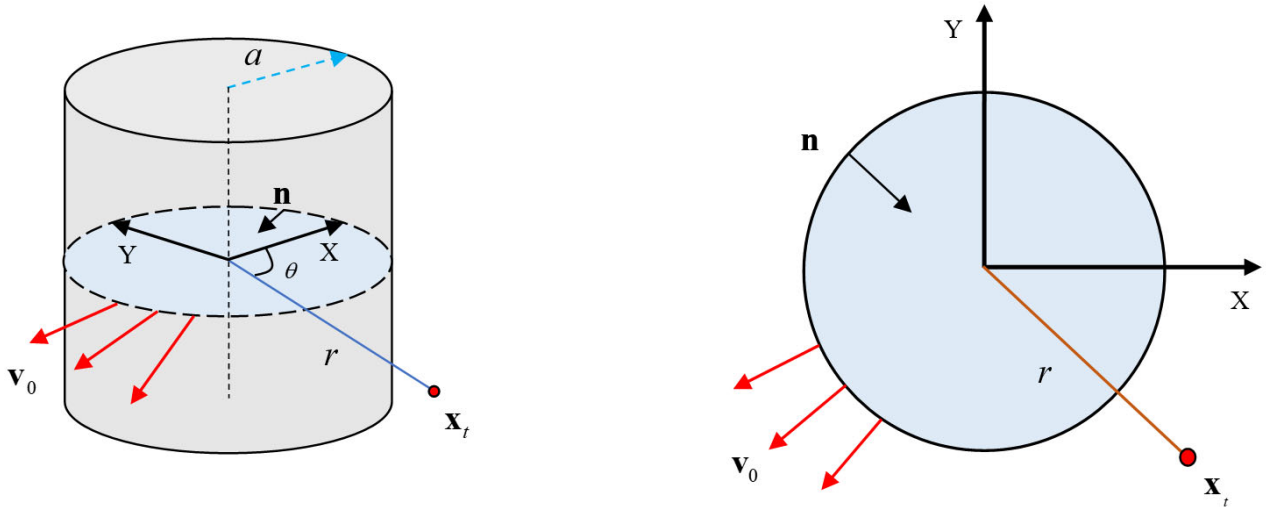

(**a**) (**b**)

Figure 1. Infinite pulsating cylinder: (**a**) a pulsating cylinder; (**b**) simplified model.

Taking the wave number as the design variable, the analytical solution of the acoustic sensitivity at the test point $\boldsymbol{x}_t$ can be given by

$$\frac{\partial p_e(r)}{\partial k} = \frac{-\mathrm{i}\rho c v_0}{\left(H_1^1(ka)\right)^2}\left[rH_1^1(kr)H_1^1(ka) + \frac{a}{2}H_0^1(kr)\left(H_0^1(ka) - H_2^1(ka)\right)\right] \tag{33}$$

where $v_0 = 1$ m/s(Neumann boundary condition); H_0^1 and H_1^1 are first-kind zero-order and one-order Hankel functions, respectively; and r is the distance between the test point and the center of cylinder.

Firstly, we investigate the influence of compression accuracy on calculation results. Figure 2 displays error curves of sound pressure sensitivity at the test point $\mathbf{x}_t = (3, 3)$ under various values of ID ($\varepsilon = 10^{-4}$, $\varepsilon = 10^{-7}$, and $\varepsilon = 10^{-10}$). In this calculation, the range of the design variable is fixed at 5~6, and the traditional BM-SBM solutions are used for an intuitive comparison. We can see from Figure 2 that the numerical error of the RSF-BM-SBM increases with a decreasing value of ID. When $\varepsilon = 10^{-10}$, the calculation accuracy is basically consistent with the traditional BM-SBM. Therefore, the higher compression accuracy should be chosen to obtain accurate and reliable results.

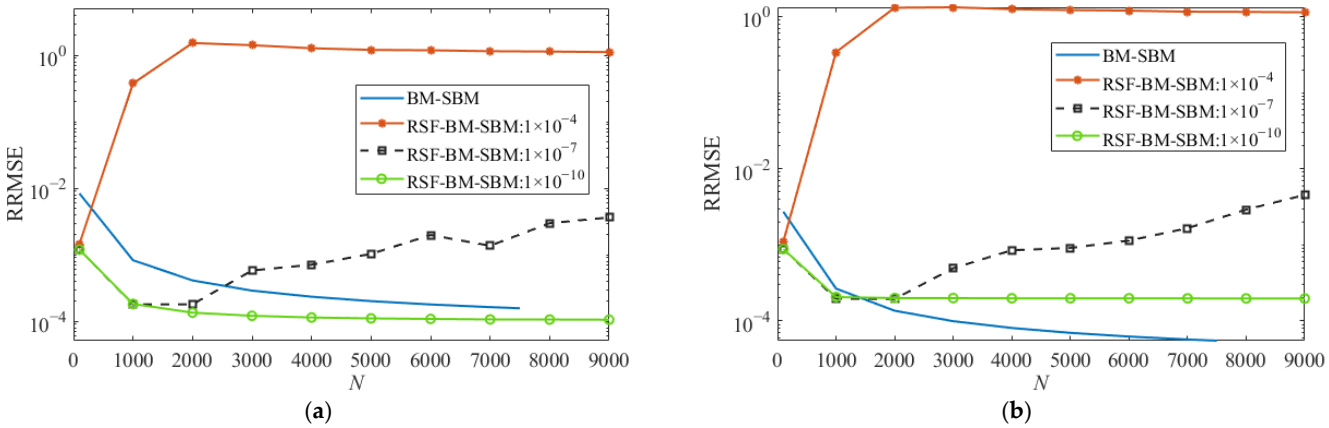

(**a**) (**b**)

Figure 2. The RRMSEs of the RSF-BM-SBM and conventional BM-SBM: (**a**) real part; (**b**) imaginary part.

In addition, Figure 3 compares the computation times of the RSF-BM-SBM and the BM-SBM under different numbers of nodes. When the number of nodes is small, both the BM-SBM and the RSF-BM-SBM consume less time. However, with an increasing number of nodes, the RSF-BM-SBM requires significantly less time than the BM-SBM.

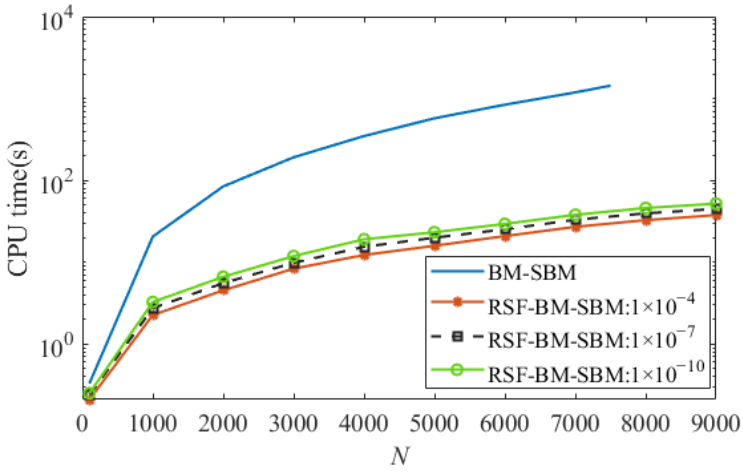

Figure 3. Comparison of CPU computation times under different numbers of nodes.

4.2. Example 2

In this example, we consider a 3D sound radiation problem on a pulsating sphere [48] with radius $a = 0.1$ m, as shown in Figure 4. This acoustic sensitivity analysis takes the wave number k as the design variable. The analytical solution of the acoustic sensitivity is

$$\frac{\partial p_e(r)}{\partial k} = \frac{\mathrm{i}\rho c v_0 a^2 e^{\mathrm{i}k(r-a)}}{r(1-\mathrm{i}ka)^2}\left[(1-\mathrm{i}ka)^2 + \mathrm{i}kr(1-\mathrm{i}ka) + \mathrm{i}ka\right] \tag{34}$$

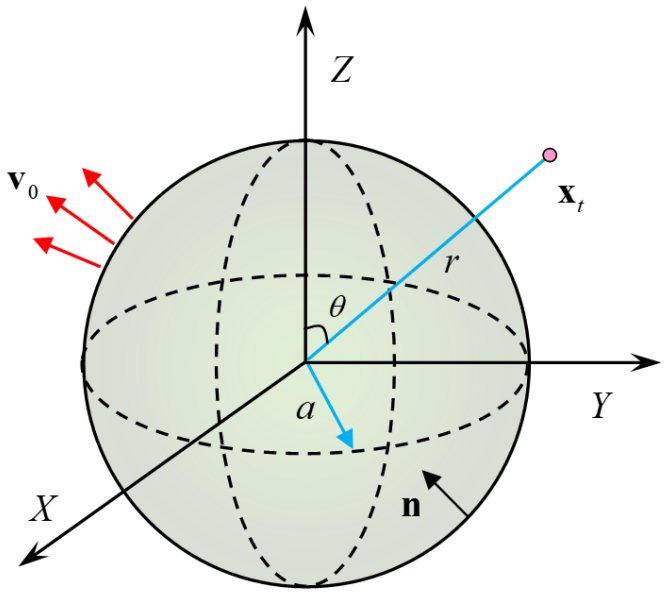

Figure 4. Acoustic radiation from a pulsating sphere.

Table 1 lists the condition numbers and the GPU memories of the conventional BM-SBM and the RSF-BM-SBM with various numbers of nodes. When the number of nodes increases, the memory required by the traditional BM-SBM increases rapidly. Therefore, when the number of nodes increases to a certain number, there will be a problem of

insufficient memory. The RSF-BM-SBM requires less memory than the BM-SBM. The traditional BM-SBM will fail when the number of boundary nodes exceeds 10,000, due to the limitation of computer memory. In addition, it should be noted that the condition number is better when using fewer nodes. As the number of nodes increases, the condition number also increases.

Table 1. Memory and condition number of the RSF-BM-SBM and the BM-SBM with various numbers of nodes.

Boundary Nodes N	Condition Number	Memory (MB)	
		Conventional BM-SBM	RSF-BM-SBM (ID: 1×10^7)
100	22.94	0.16	0.32
2000	104.37	64.00	107.82
4000	1.50×10^7	256.00	239.01
7500	3.33×10^7	900.00	530.60
9000	2.79×10^8	1296.00	589.31
58,204	——	——	6772.86
112,722	——	——	14,541.76
150,082	——	——	27,069.25

4.3. Example 3

The last example considers a scaled-down vehicle model, as shown in Figure 5. This is an acoustic scattering problem, and but there is no analytical solution for sound pressure and sensitivity. Due to the complexity of the model, a large number of boundary points need to be configured, and the traditional BM-SBM cannot be calculated, so the acoustic sensitivity of the model is established by applying the RSF-BM-SBM involving 104,896 source points. In this model, a unit amplitude plane wave of wavenumber $k = 4$ propagates in the positive x-axis direction.

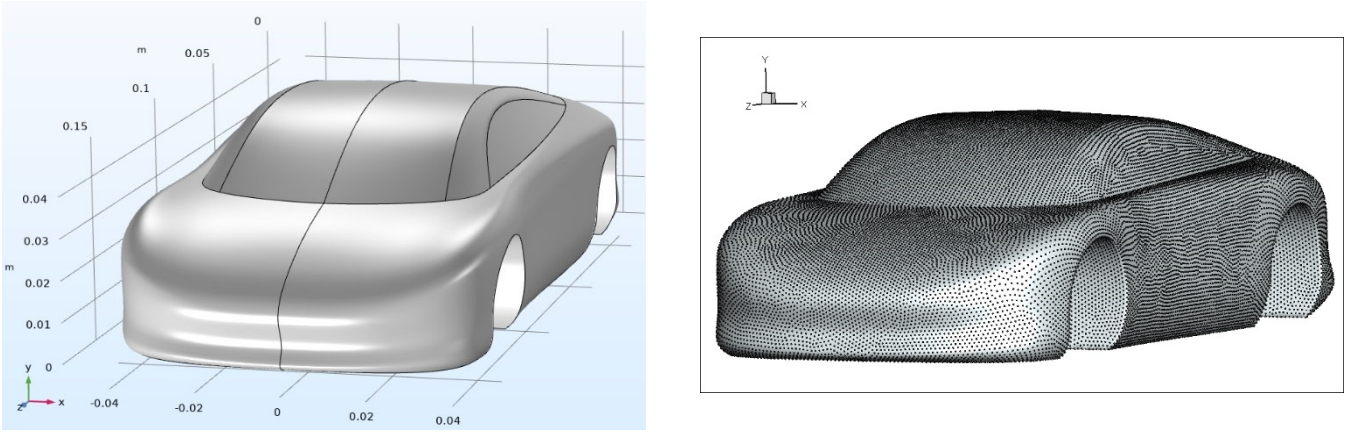

(**a**) (**b**)

Figure 5. An irregular rigid vehicle model boundary point configuration ($N = 104,896$): (**a**) vehicle model; (**b**) boundary points.

Firstly, we chose a spherical surface with radius $r = 1$ m in order to test the accuracy of the proposed method in solving the acoustic scattering of this complex structure. The RSF-BM-SBM and COMSOL Multiphysics FEM solver were used to calculate the scattered sound pressure levels on the surface. The FEM needs to set a perfectly matched layer when solving this kind of problem. Numerical results in Figure 6 indicate the capability and reliability of the proposed method for the 3D complex structure.

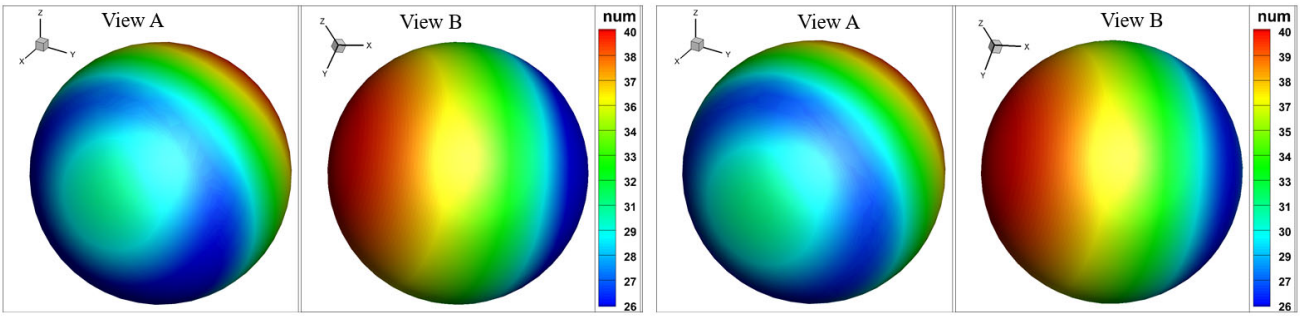

(**a**) (**b**)

Figure 6. Distributions of the scattered sound pressure level on the investigated surface obtained by using the FEM and RSF-BM-SBM: (**a**) FEM; (**b**) RSF-BM-SBM.

We intercepted a limited domain around the car body as shown in Figure 7, and the distributions of sensitivity values with respect to the design variable k were computed by the RSF-BM-SBM. Figure 8 shows the amplitudes of sound pressure sensitivity under different wave numbers. Obvious differences can be observed, which provides a reference for the analysis of acoustic sensitivity of complex structures.

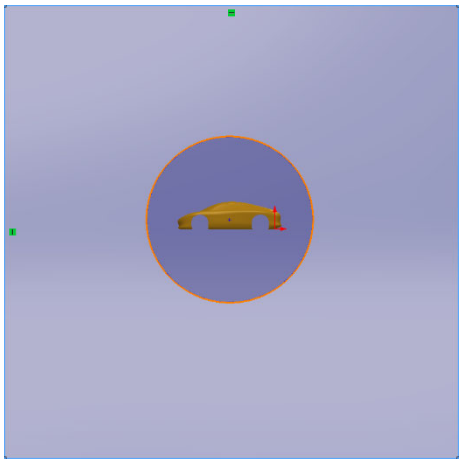

Figure 7. Distributions of boundary source points and test points.

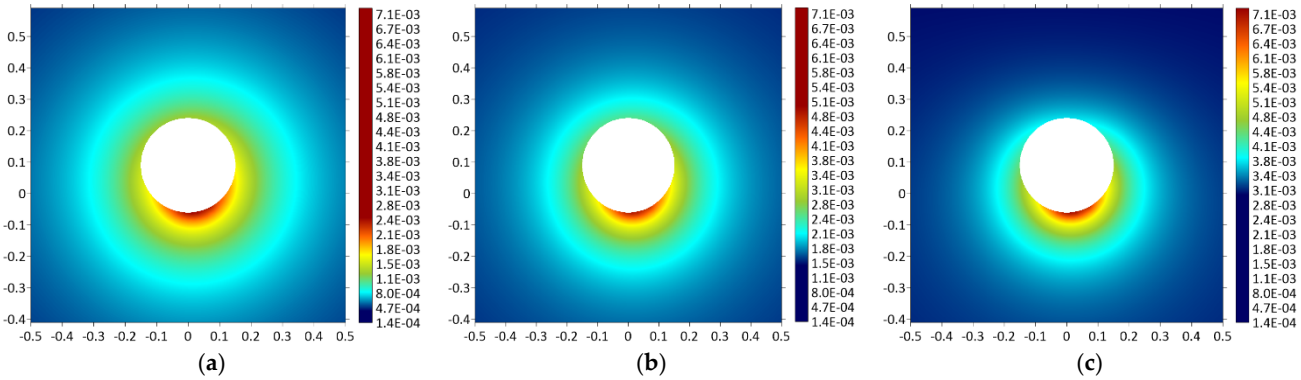

(**a**) (**b**) (**c**)

Figure 8. Acoustic pressure sensitivities ($|\partial p/\partial k|$) on $\{(x, y, z,)|-0.5 \leq y \leq 0.5,\ -0.4 \leq z \leq 0.6, x = 0\}$ cross section under different values of k: (**a**) $k = 3$; (**b**) $k = 6$; (**c**) $k = 9$.

5. Conclusions

In this paper, a fast RSF-BM-SBM has been developed for the acoustic sensitivity analysis of 2D and 3D domains. The present scheme is an accurate and semi-analytical

method with the merits of being truly meshless, integration free, mathematically simple, and easy to program. As a boundary-type method based on the fundamental solution, the RSF-BM-SBM is straightforward for addressing exterior acoustic problems encountered in acoustic design sensitivity analysis. In addition, the fictitious frequency issue has been successfully overcome by using the Burton–Miller formulation. Compared with previous approaches [48,49], the proposed fast RSF-BM-SBM greatly reduces the computation time and improves the computation scale by introducing the RSF technique, which makes it possible for the method to analyze the acoustic sensitivity of high-dimensional and large-scale structures.

Through investigating the acoustic scattering problem of an infinite pulsating cylinder, the RSF-SM-SBM shows obvious advantages in solving large-scale problems. Under high compression accuracy (ID: $\varepsilon = 10^{-10}$), the CPU computation time of the RSF-SM-SBM is much shorter than that of the BM-SBM, while the calculation accuracy is basically the same. Numerical results for sound radiation from a pulsating sphere demonstrate that the traditional BM-SBM has a huge demand for memory, which limits its application in large-scale problems. Conversely, the RSF-BM-SBM has significant advantages in reducing computation time and computation cost. For the acoustic sensitivity analysis of a car-like structure, the proposed scheme is also applicable, which indicates the ability and potential of the fast method for 3D complex geometries.

Author Contributions: Conceptualization, L.L. and F.W.; Investigation, X.S. and C.Y.; Methodology, W.L. and F.W.; Resources, S.C.; Supervision, C.Y.; Validation, L.L.; Writing—original draft, S.C.; Writing—review & editing, X.S., W.L., C.Y. and F.W. All authors have read and agreed to the published version of the manuscript.

Funding: The work described in this paper was supported by the National Natural Science Foundation of China (No. 11802151).

Data Availability Statement: Not applicable.

Conflicts of Interest: The authors declare no conflict of interest.

References

1. Gohari, H.; Zarastvand, M.; Talebitooti, R.; Loghmani, A.; Omidpanah, M. Radiated sound control from a smart cylinder sub-jected to piezoelectric uncertainties based on sliding mode technique using self-adjusting boundary layer. *Aerosp. Sci. Technol.* **2020**, *106*, 106141. [CrossRef]
2. Xu, M.; Du, J.; Wang, C.; Li, Y. Hybrid uncertainty propagation in structural-acoustic systems based on the polynomial chaos expansion and dimension-wise analysis. *Comput. Methods Appl. Mech. Eng.* **2017**, *320*, 198–217. [CrossRef]
3. Rahmatnezhad, K.; Zarastvand, M.; Talebitooti, R. Mechanism study and power transmission feature of acoustically stimu-lated and thermally loaded composite shell structures with double curvature. *Compos. Struct.* **2021**, *276*, 114557. [CrossRef]
4. Chen, Q.; Fei, Q.; Wu, S.; Li, Y. Uncertainty propagation of the energy flow in vibro-acoustic system with fuzzy parameters. *Aerosp. Sci. Technol.* **2019**, *94*, 105367. [CrossRef]
5. Shojaei, A.; Mossaiby, F.; Zaccariotto, M.; Galvanetto, U. A local collocation method to construct Dirichlet-type absorbing boundary conditions for transient scalar wave propagation problems. *Comput. Methods Appl. Mech. Eng.* **2019**, *356*, 629–651. [CrossRef]
6. Zarastvand, M.R.; Ghassabi, M.; Talebitooti, R. Prediction of acoustic wave transmission features of the multilayered plate constructions: A review. *J. Sandw. Struct. Mater.* **2022**, *24*, 218–293. [CrossRef]
7. Shojaei, A.; Hermann, A.; Seleson, P.; Cyron, C. Dirichlet absorbing boundary conditions for classical and peridynamic diffu-sion-type models. *Comput. Mech.* **2020**, *66*, 773–793. [CrossRef]
8. Scarpa, F. Parametric Sensitivity Analysis of Coupled Acoustic-Structural Systems. *J. Vib. Acoust.* **2000**, *122*, 109–115. [CrossRef]
9. Dong, J.; Choi, K.K.; Wang, A.; Zhang, W.; Vlahopoulos, N. Parametric design sensitivity analysis of high-frequency structur-al-acoustic problems using energy finite element method. *Int. J. Numer. Methods Eng.* **2005**, *62*, 83–121. [CrossRef]
10. Chai, Y.; Li, W.; Liu, Z. Analysis of transient wave propagation dynamics using the enriched finite element method with interpolation cover functions. *Appl. Math. Comput.* **2022**, *412*, 126564. [CrossRef]
11. Koo, B.-U.; Ih, J.-G.; Lee, B.-C. Acoustic shape sensitivity analysis using the boundary integral equation. *J. Acoust. Soc. Am.* **1998**, *104*, 2851–2860. [CrossRef]
12. Kane, J.H.; Mao, S.; Everstine, G.C. A boundary element formulation for acoustic shape sensitivity analysis. *J. Acoust. Soc. Am.* **1991**, *90*, 561–573. [CrossRef]
13. Belytschko, T.; Lu, Y.; Gu, L. Element-free Galerkin methods. *Int. J. Numer. Methods Eng.* **1994**, *37*, 229–256. [CrossRef]

14. Lu, Y.; Belytschko, T.; Gu, L. A new implementation of the element free Galerkin method. *Comput. Methods Appl. Mech. Eng.* **1994**, *113*, 397–414. [CrossRef]
15. Shojaei, A.; Boroomand, B.; Soleimanifar, E. A meshless method for unbounded acoustic problems. *J. Acoust. Soc. Am.* **2016**, *139*, 2613–2623. [CrossRef] [PubMed]
16. Mossaiby, F.; Shojaei, A.; Boroomand, B.; Zaccariotto, M.; Galvanetto, U. Local Dirichlet-type absorbing boundary conditions for transient elastic wave propagation problems. *Comput. Methods Appl. Mech. Eng.* **2020**, *362*, 112856. [CrossRef]
17. Chen, Z.; Wang, F. Localized Method of Fundamental Solutions for Acoustic Analysis Inside a Car Cavity with Sound-Absorbing Material. *Adv. Appl. Math. Mech.* **2022**. [CrossRef]
18. Chen, Z.; Wang, F.; Cheng, S.; Wu, G. Localized MFS for three-dimensional acoustic inverse problems on complicated do-mains. *Int. J. Mech. Syst. Dyn.* **2022**, *2*, 143–152. [CrossRef]
19. Wang, F.; Gu, Y.; Qu, W.; Zhang, C. Localized boundary knot method and its application to large-scale acoustic problems. *Comput. Methods Appl. Mech. Eng.* **2020**, *361*, 112729. [CrossRef]
20. Fairweather, G.; Karageorghis, A. The method of fundamental solutions for elliptic boundary value problems. *Adv. Comput. Math.* **1998**, *9*, 69–95. [CrossRef]
21. Poullikkas, A.; Karageorghis, A.; Georgiou, G. The method of fundamental solutions for three-dimensional elastostatics problems. *Comput. Struct.* **2002**, *80*, 365–370. [CrossRef]
22. Chen, W. Singular boundary method: A novel, simple, meshfree, boundary collocation numerical method. *Chin. J. Solid Mech.* **2009**, *30*, 592–599.
23. Burton, A.J.; Miller, G.F. The application of integral equation methods to the numerical solution of some exterior boundary-value problems. *Proc. R. Soc. London. Ser. A Math. Phys. Sci.* **1971**, *323*, 201–210. [CrossRef]
24. Fu, Z.-J.; Chen, W.; Gu, Y. Burton–Miller-type singular boundary method for acoustic radiation and scattering. *J. Sound Vib.* **2014**, *333*, 3776–3793. [CrossRef]
25. Li, J.; Chen, W. A modified singular boundary method for three-dimensional high frequency acoustic wave problems. *Appl. Math. Model.* **2018**, *54*, 189–201. [CrossRef]
26. Qu, W.; Zheng, C.; Zhang, Y.; Gu, Y.; Wang, F. A wideband fast multipole accelerated singular boundary method for three-dimensional acoustic problems. *Comput. Struct.* **2018**, *206*, 82–89. [CrossRef]
27. Wei, X.; Luo, W. 2.5D singular boundary method for acoustic wave propagation. *Appl. Math. Lett.* **2021**, *112*, 106760. [CrossRef]
28. Gu, Y.; Chen, W.; He, X. Singular boundary method for steady-state heat conduction in three dimensional general anisotropic media. *Int. J. Heat Mass Transf.* **2012**, *55*, 4837–4848. [CrossRef]
29. Wei, X.; Sun, L.; Yin, S.; Chen, B. A boundary-only treatment by singular boundary method for two-dimensional inhomogeneous problems. *Appl. Math. Model.* **2018**, *62*, 338–351. [CrossRef]
30. Li, W.; Chen, W. Band gap calculations of photonic crystals by singular boundary method. *J. Comput. Appl. Math.* **2017**, *315*, 273–286. [CrossRef]
31. Cheng, A.H.; Hong, Y. An overview of the method of fundamental solutions—Solvability, uniqueness, convergence, and stability. *Eng. Anal. Bound. Elem.* **2020**, *120*, 118–152. [CrossRef]
32. Karageorghis, A.; Johansson, B.; Lesnic, D. The method of fundamental solutions for the identification of a sound-soft obstacle in inverse acoustic scattering. *Appl. Numer. Math.* **2012**, *62*, 1767–1780. [CrossRef]
33. Jin, B.; Zheng, Y. Boundary knot method for some inverse problems associated with the Helmholtz equation. *Int. J. Numer. Methods Eng.* **2005**, *62*, 1636–1651. [CrossRef]
34. Zheng, C.; Matsumoto, T.; Takahashi, T.; Chen, H. A wideband fast multipole boundary element method for three dimensional acoustic shape sensitivity analysis based on direct differentiation method. *Eng. Anal. Bound. Elem.* **2012**, *36*, 361–371. [CrossRef]
35. Chen, L.; Liu, L.; Zhao, W.; Chen, H. 2D Acoustic Design Sensitivity Analysis Based on Adjoint Variable Method Using Different Types of Boundary Elements. *Acoust. Aust.* **2016**, *44*, 343–357. [CrossRef]
36. Xu, Y.; Zhao, W.; Chen, L.; Chen, H. Distribution Optimization for Acoustic Design of Porous Layer by the Boundary Element Method. *Acoust. Aust.* **2020**, *48*, 107–119. [CrossRef]
37. Liu, Y.; Nishimura, N.; Yao, Z. A fast multipole accelerated method of fundamental solutions for potential problems. *Eng. Anal. Bound. Elem.* **2005**, *29*, 1016–1024. [CrossRef]
38. Zheng, C.; Zhao, W.; Gao, H.; Du, L.; Zhang, Y.; Bi, C. Sensitivity analysis of acoustic eigenfrequencies by using a boundary element method. *J. Acoust. Soc. Am.* **2021**, *149*, 2027–2039. [CrossRef]
39. Godinho, L.; Soares, D.; Santos, P. Efficient analysis of sound propagation in sonic crystals using an ACA–MFS approach. *Eng. Anal. Bound. Elem.* **2016**, *69*, 72–85. [CrossRef]
40. Qu, W.; Chen, W.; Gu, Y. Fast multipole accelerated singular boundary method for the 3D Helmholtz equation in low frequency regime. *Comput. Math. Appl.* **2015**, *70*, 679–690. [CrossRef]
41. Qu, W.; Chen, W.; Zheng, C. Diagonal form fast multipole singular boundary method applied to the solution of high-frequency acoustic radiation and scattering. *Int. J. Numer. Methods Eng.* **2017**, *111*, 803–815. [CrossRef]
42. Wei, X.; Chen, B.; Chen, S.; Yin, S. An ACA-SBM for some 2D steady-state heat conduction problems. *Eng. Anal. Bound. Elem.* **2016**, *71*, 101–111. [CrossRef]
43. Li, W.; Chen, W.; Fu, Z. Precorrected-FFT Accelerated Singular Boundary Method for Large-Scale Three-Dimensional Potential Problems. *Commun. Comput. Phys.* **2017**, *22*, 460–472. [CrossRef]

44. Li, W. A fast singular boundary method for 3D Helmholtz equation. *Comput. Math. Appl.* **2019**, *77*, 525–535. [CrossRef]
45. Li, W.; Wang, F. Precorrected-FFT Accelerated Singular Boundary Method for High-Frequency Acoustic Radiation and Scattering. *Mathematics* **2022**, *10*, 238. [CrossRef]
46. Li, W.; Xu, S.; Shao, M. Simulation of two-dimensional steady-state heat conduction problems by a fast singular boundary method. *Eng. Anal. Bound. Elem.* **2019**, *108*, 149–157. [CrossRef]
47. Li, W.; Wu, B. A fast direct singular boundary method for three-dimensional potential problems. *Eng. Anal. Bound. Elem.* **2022**, *139*, 132–136. [CrossRef]
48. Cheng, S.; Wang, F.; Wu, G.; Zhang, C. A semi-analytical and boundary-type meshless method with adjoint variable formulation for acoustic design sensitivity analysis. *Appl. Math. Lett.* **2022**, *131*, 108068. [CrossRef]
49. Cheng, S.; Wang, F.; Li, P.-W.; Qu, W. Singular boundary method for 2D and 3D acoustic design sensitivity analysis. *Comput. Math. Appl.* **2022**, *119*, 371–386. [CrossRef]
50. Ho, K.L.; Greengard, L. A Fast Direct Solver for Structured Linear Systems by Recursive Skeletonization. *SIAM J. Sci. Comput.* **2012**, *34*, A2507–A2532. [CrossRef]
51. Ho, K.L.; Ying, L. Hierarchical Interpolative Factorization for Elliptic Operators: Differential Equations. *Commun. Pure Appl. Math.* **2016**, *69*, 1415–1451. [CrossRef]
52. Xing, W.; Wen, C.; Sun, L.; Chen, B. A simple accurate formula evaluating origin intensity factor in singular boundary method for two-dimensional potential problems with Dirichlet boundary. *Eng. Anal. Bound. Elem.* **2015**, *58*, 151–165.
53. Li, J.; Chen, W.; Fu, Z.; Sun, L. Explicit empirical formula evaluating original intensity factors of singular boundary method for potential and Helmholtz problems. *Eng. Anal. Bound. Elem.* **2016**, *73*, 161–169. [CrossRef]
54. Cheng, H.; Gimbutas, Z.; Martinsson, P.G.; Rokhlin, V. On the Compression of Low Rank Matrices. *SIAM J. Sci. Comput.* **2005**, *26*, 1389–1404. [CrossRef]